A Scalable port-Hamiltonian Model for Incompressible Fluids in Irregular Geometries

Luis A. Mora * **Héctor Ramírez** * **Juan I. Yuz** *
Yann Le Gorrec **

_* Department of Electronic Engineering, Universidad Técnica Federico
Santa María, Av. España 1680 Valparaíso, Chile (e-mail:
luis.moraa@sansano.usm.cl, hector.ramirez@usm.cl, juan.yuz@usm.cl).
** FEMTO-ST, Univ. Bourgogne Franche-Comté, CNRS, 24 rue
Savary, F-2500 Besançon, France (e-mail: yann.le.gorrec@ens2m.fr)_

Abstract: The behavior of fluids in channel with irregular geometries is study through the partial differential equations that describe mass and momentum balances using numerical methods. In this paper, from these partial differential equations, we obtain a scalable lumped-parameter model to describe the behavior of incompressible fluids in channels with sudden changes in cross sectional areas, including dissipative effects, using the port-Hamiltonian framework. We relax the incompressibility hypothesis to admit density variations in an infinitesimal section in the coupling zone between two sections. Simulation results with airflow shows how the proposed model allows an analysis of the fluid in each section of fluid channel and reproduce a suitable flow behavior where density variations in coupling zones are less than 0.6%

Keywords: Incompressible fluids, port-Hamiltonian framework, irregular geometry, scalable lumped-parameter model

1. INTRODUCTION

A fluid is considered incompressible when its density is constant. In the practice, to simplify the analysis of complex systems, is common consider as incompressible any fluid whose density variation is very little, i.e., can be considered as negligible. The incompressibility approximation depends on the conditions to which the fluid is subjected (Johnson, 1998). In an adiabatic process the flow of either a gas or a liquid can be considered incompressible when its Mach number, ratio between the fluid and sound velocities, is very small. A particular case highly studied is the air, that can be considered incompressible for Mach numbers less than 0.3. This assumption for the airflow is usual in aerospace engineering (Wu and Cao, 2015), and bioengineering applications (Comer et al., 2001; Cal et al., 2017).

Consider a fluid in motion through a channel width irregular geometry, as shown Figure 1, where the cross-sectional area varies in different sections. Changes in the cross-sectional area produces variations in the flow speed and energy losses associated width the channel expansion and contraction. This system can be found in industrial process as wastewater treatment (Hager, 2010), and bioengineering applications as the study of arterial blood flow (Guidoboni et al., 2009) and airflow in the vocal apparatus (Cisonni et al., 2008). The fluid behav-
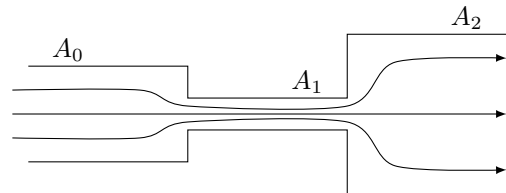
Fig. 1. Fluid through a channel with irregular geometry

ior in irregular geometries is commonly studied through distributed-parameters models. These models use numerical techniques, as finite-volumes and LS-STAG, among others, that presents strong computational demands to obtain a detailed flow description (Bourantas et al., 2016; Sharatchandra and Rhode, 1994; Darbandi and Naderi, 2006).

To reduce the complexity of fluid systems, a common engineering simplification is to consider the fluid as an one-dimensional flow. Thus, the fluid behavior is given by following partial differential equations (PDEs):

$$\partial_t \rho + \partial_z (\rho v) = 0 \tag{1}$$

$$\rho \partial_t v + \frac{\rho}{2} \partial_z v^2 + \partial_z p = 0 \tag{2}$$

where ρ and v are the fluid density and velocity, p is the static pressure and $\partial_z = \partial/\partial z$. The PDEs in (1) and (2) represents the mass and momentum conservation laws for fluids (Bird et al., 2014), receptively.

Additionally, to simplify the computational complexity lumped-parameter models are used. In these models the
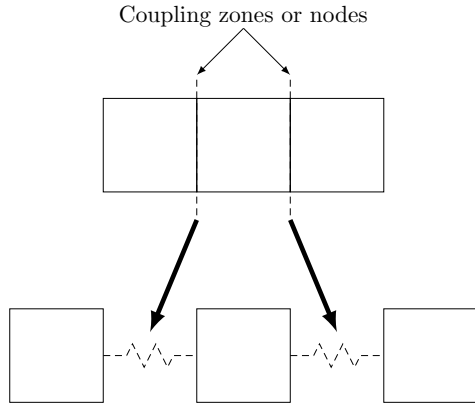
Fig. 2. Interconnection of masses in mechanical systems

flow behavior is studied only in one section of the channel. Now, consider that the flow channel is divided in n sections through $n-1$ coupling zones or nodes. Under the incompressibility hypothesis, obtaining a model that allows to analyze the flow behavior presents drawbacks associated with causality problems. To illustrate these drawbacks consider the mechanical system of three masses that shown in Figure 2. If we coupling masses directly, the resulting model is represented by a single mass equivalent to the sum of individual masses. To obtain a model that describe the behavior of each mass is necessary the use of an additional element, a spring, to coupling, obtaining a model where the behavior of each mass can be individually analyze. In a fluid, the model that describe the flow in each section is equivalent to a mass in a mechanical system, then in each node we need a element that permit a proper coupling between sections.

On the other hand, the port-Hamiltonian (PH) framework is a useful mathematical tool to model systems (Van der Schaft and Jeltsema, 2014). This framework is focused on describing the energy flux in the system and provide a set of advantageous features. In a PH model the inputs $u \in \mathbb{R}^m$ and outputs $y \in \mathbb{R}^m$ are conjugated in the power sense, i.e., the inner product between u and y represents the supply power. Additionally, the PH models describe the state variables as a function of a non-negative function H that represents the total storage energy in the system and whose rate of change is bounded by the power supplied, $\dot{H} \leq y^T u$. This feature provide properties of the control theory as passivity and Lyapunov stability (Van der Schaft, 2017).

In general, using the PH framework a lumped-parameter system of n state variables can be describe as

$$\dot{x} = (J - R)\partial_x H + gu \qquad (3)$$
$$y = g^T \partial_x H \qquad (4)$$

where $J \in \mathbb{R}^{n \times n}$ is an interconnection matrix, $R \in \mathbb{R}^{n \times n}$ is the dissipation matrix and $g \in \mathbb{R}^{n \times m}$ is the input matrix.

The behavior of fluids using a infinite-dimensional port-Hamiltonian formulation has been studied in works as van der Schaft and Maschke (2002); Morrison (1998); Morrison et al. (2009); Altmann and Schulze (2017). However to simulate these model is necessary apply spatial discretization methods. In this sense, in works as Kotyczka (2013); Kotyczka and Maschke (2017); Trenchant et al.
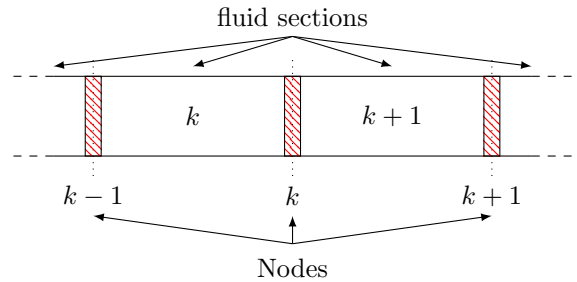
Fig. 3. Coupling incompressible fluid sections using a compressible behavior in nodes

(2018a,b) has been proposed spatial discretization techniques to preserve the port-Hamiltonian structure.

From a PH view point, a mass and a spring are element that storage kinetic and potential energies, respectively (Van der Schaft and Jeltsema, 2014). In a incompressible flow, under adiabatic conditions and neglecting the gravitational effects, the fluid storage only kinetic energy, i.e., the incompressibility hypothesis restricts the storage of potential energy in the fluid.

In this paper we propose a scalable port-Hamiltonian model to describe the behavior of incompressible fluids in irregular geometries. For this we consider relax the incompressible hypothesis to obtain a proper coupling between fluid sections.

2. A SIMPLE MODEL FOR THE INCOMPRESSIBLE FLUID

To obtain a fluid element equivalent to a springs, is necessary to consider how the potential energy storages in a fluid. Neglecting the gravitational effects and considering a isothermal fluid, the potential energy can be associated with the fluid work. However, under the incompressibility assumption the fluid work is zero. Thus, to relax the incompressible hypothesis we consider the following assumptions

Assumption 1. Let a fluid whose density varies so little, $\Delta \rho \lll \rho$. Thus, we can consider the flow in one section behaves as an incompressible fluid and the compressibility effects occur in an infinitesimal volume, called node, located between 2 sections, as shown in Figure 3.

Assumption 2. As a node represent an infinitesimal volume in the coupling zone between two fluid sections, when the node expands or contracts, the mass variations are much less than the volume variations. Then, we consider an uniform density distribution and a constant mass in each node, i.e., the following relationship is satisfied

$$\rho_j V_j = \kappa \qquad (5)$$

where ρ_j and V_j are the density and volume in node j.

2.1 Modeling a fluid section

The balance equation in (2) represents the momentum conservation law without losses. However, when the fluid channel presents variations in its geometry, as contraction, expansion and direction changes, is know that occur energy losses in the flow (Brodkey and Hershey, 2003; Villegas-León et al., 2016). These losses are given by local

turbulences that contribute significantly to the pressure drop. Thus, to including this effects and considering the incompressibility assumption, we rewrite the momentum balance as

$$\rho_0 \partial_t v = -\partial_z P - f_d(z) \tag{6}$$

where ρ_0 is the reference fluid density, $P = \frac{1}{2}\rho_0 v^2 + p$ is the total pressure field and $f_d(z)$ is a force associated with mechanical energy losses.

Integrating (6) in the corresponding volume of section i, using the Leibnitz integral rule, the Gauss divergence theorem and considering an uniform cross-sectional area in the section, we can obtain a finite-dimensional description of the fluid as follow

$$\int \rho_0 \partial_t v dV_i = -\int \partial_z P dV_i - \int f_d(z) dV_i \tag{7a}$$

$$\rho_0 \frac{d}{dt} \int v dV_i = \int P dS_{1i} - \int P dS_{2i} - A_i \int f_d(z) dz \tag{7b}$$

$$\rho_0 V_i \dot{v}_i = A_i P_{1i} - A_i P_{2i} - A_i \int f_d(z) dz \tag{7c}$$

where $\dot{v}_i$ is the time derivative of the average velocity in section i, A_i is the cross-sectional area, and P_{1i} and P_{2i} are the average pressures of the inlet and outlet boundary surfaces S_{1i} and S_{2i} respectively.

According to Mulley (2004) the loss of mechanical energy in channel contractions and expansions has been empirically associated with the dynamical pressure of the fluid. Thus, in a volume V_i we use the following approximation:

$$\int f_d(z) dz \approx \lambda_i \frac{1}{2} \rho_0 v_i^2 \tag{8}$$

where the term $(\rho_0/2)\lambda_i v_i^2$ is the average pressure drop associated with the mechanical energy losses and λ_i is a dimensionless loss factor in section i. Substituting (8) in (7c), we can describe the dynamic behavior of the fluid in a section as

$$\rho_0 V_i \dot{v}_i = -A_i \frac{\rho_0}{2} \lambda_i v_i^2 + A_i P_{1i} - A_i P_{2i} \tag{9}$$

Defining $\pi_i = \rho_0 V_i v_i$ as the air momentum in section i and $K_i = \frac{1}{2}C_{xi}\pi_i^2$ as the corresponding kinetic energy, where $C_{xi} = 1/(\rho_0 V_i)$, the port-Hamiltonian formulation of (9) is given by

$$\dot{\pi}_i = -A_i \frac{\rho_0 \lambda_i \pi_i}{2V_i} \partial_{\pi_i} K_i + \begin{bmatrix} A_i & -A_i \end{bmatrix} \begin{bmatrix} P_{1i} \\ P_{2i} \end{bmatrix} \tag{10a}$$

$$\begin{bmatrix} Q_{1j} \\ -Q_{2j} \end{bmatrix} = \begin{bmatrix} A_i \\ -A_i \end{bmatrix} \partial_{\pi_i} K_i \tag{10b}$$

where Q_{1i} and Q_{2i} are the inlet and outlet volumetric flows in section i. The definition of loss factor λ_i depends of geometry changes in the channel and will be discussed below.

2.2 Modeling the nodes

The model proposed in (10) represents the fluid behavior on arbitrary section i. However, note that the input and output ports are not compatible to interconnect width adjacent sections. This drawback is a consequence of the causality problem above discussed.

To solve this obstacle, we use the Assumption 1 to obtain a model in the coupling zone between two fluid sections. Thus, conservation mass law in (1) can be rewritten as

$$\partial_t \rho_j = -\rho_j \partial_z v_j \tag{11}$$

Integrating (11) in the volume of node j and using the Gauss divergence theorem, the model that describe the fluid behavior in a node can be deduced as follow

$$\int_{V_j} \partial_t \rho_j dV_j = -\rho_j \int_{V_j} \partial_z v_j dV_j \tag{12a}$$

$$V_j \dot{\rho}_j = \rho_j \left(\int v_j dS_1 j - \int v_j dS_2 j \right) \tag{12b}$$

$$\dot{\rho}_j = \frac{\rho_j}{V_j} \left(Q_{1j} - Q_{2j} \right) \tag{12c}$$

where the Q_{1j} and Q_{2j} are the average flows in the inlet and outlet cross-sectional surfaces, S_{1j} and S_{2j}, of the corresponding node, respectively.

Note that the inputs ports in (12c) are compatible with the outputs ports of adjacent fluid sections described by (10). To complete the coupling is necessary obtain a expression to relate the node pressure changes with the corresponding density variations. Then, given the constant mas hypothesis described in Assumption 2, we can use the bulk modulus definition [cite], $\beta_S = -V_j(dp_j/dV_j)$, and (5) to write the differential of pressure in a node as

$$dp_j = \frac{\beta_S}{\rho_j} d\rho_j \tag{13}$$

Considering that $p_j = 0$ when $\rho_j = \rho_0$ and solving (13), the pressure behavior in the j-th node is given by

$$p_j(\rho_j) = \beta_S \ln \left(\frac{\rho_j}{\rho_0} \right) \tag{14}$$

Given the infinitesimal volume assumption, the kinetic energy in the node can be neglected. Thus, the energy in an arbitrary node j, is is given by the potential energy associated with the corresponding density variations. From the first law of thermodynamics [cite] and considering an adiabatic process, the potential energy in node j, E_j, is given by the fluid work, $dE_j = -p_j dV_j$. Using (5), the differential of potential energy can be written as

$$dE_j = p_j \frac{\kappa}{\rho_j^2} d\rho_j \tag{15}$$

where p_j is the node pressure. From (15), the pressure in node j can be described as $p_j = (\rho_j^2/\kappa)\partial_{\rho_j} E_j$. Then, the behavior potential energy is given by the following non-negative function

$$E_j(\rho_j) = \kappa \beta_S \left(\frac{\rho_j - \rho_0 \left(1 + \ln(\rho_j/\rho_0) \right)}{\rho_j \rho_0} \right) \tag{16}$$

Finally, using (16) we can rewrite (12c) as the following port-Hamiltonian formulation

$$\dot{\rho}_j = 0\partial_{\rho_j} E_j + \begin{bmatrix} \rho_j^2/\kappa & -\rho_j^2/\kappa \end{bmatrix} \begin{bmatrix} Q_{1j} \\ Q_{2j} \end{bmatrix} \tag{17a}$$

$$\begin{bmatrix} p_{1j} \\ -p_{2j} \end{bmatrix} = \begin{bmatrix} \rho_j^2/\kappa \\ -\rho_j^2/\kappa \end{bmatrix} \partial_{\rho_j} E_j \tag{17b}$$

Note that the input and outputs ports in (17) are compatible to coupling the adjacent fluid sections, i.e., this model can be used to obtain a scalable fluid model.

2.3 Overall Model

Now consider a fluid channel dived in two sections, i.e., $i \in \{1, 2\}$ and $j = 1$. Thus, from model in (10), the behavior of each fluid section are given by

$$\dot{\pi}_1 = -A_1 \frac{\rho_0 \lambda_1 \pi_1}{2V_1} \partial_{\pi_1} K_1 + [A_1 \ -A_1] \begin{bmatrix} P_{11} \\ P_{21} \end{bmatrix} \quad (18a)$$

$$\begin{bmatrix} Q_{11} \\ -Q_{21} \end{bmatrix} = \begin{bmatrix} A_1 \\ -A_1 \end{bmatrix} \partial_{\pi_i} K_1 \quad (18b)$$

$$\dot{\pi}_2 = -A_2 \frac{\rho_0 \lambda_2 \pi_2}{2V_2} \partial_{\pi_2} K_2 + [A_2 \ -A_2] \begin{bmatrix} P_{12} \\ P_{22} \end{bmatrix} \quad (19a)$$

$$\begin{bmatrix} Q_{12} \\ -Q_{22} \end{bmatrix} = \begin{bmatrix} A_2 \\ -A_2 \end{bmatrix} \partial_{\pi_2} K_2 \quad (19b)$$

where $K_1 = \frac{1}{2} C_{x1} \pi_1^2$ and $K_2 = \frac{1}{2} C_{x2} \pi_2^2$ are the kinetic energies in corresponding sections.

On the other hand, from the model in (17), the node behavior is given by

$$\dot{\rho}_1 = 0 \partial_{\rho_1} E_1 + [\rho_1^2/\kappa \ -\rho_1^2/\kappa] \begin{bmatrix} Q_{11} \\ Q_{21} \end{bmatrix} \quad (20a)$$

$$\begin{bmatrix} p_{11} \\ -p_{21} \end{bmatrix} = \begin{bmatrix} \rho_1^2/\kappa \\ -\rho_1^2/\kappa \end{bmatrix} \partial_{\rho_1} E_1 \quad (20b)$$

where $E_1 = \kappa \beta_S \left(\frac{\rho_1 - \rho_0(1 + \ln(\rho_1/\rho_0))}{\rho_1 \rho_0} \right)$.

Note that the input flows in (20) are compatible width the outputs Q_{21} in (18) and Q_{12} in (19). Similarly, the outputs in (20) are compatible width the inputs P_{21} in (18) and P_{12} in (19). Thus, we can coupling the two fluid sections using the node model and obtain the following port-Hamiltonian model to describe the fluid

$$\begin{bmatrix} \dot{\pi}_1 \\ \dot{\pi}_2 \\ \dot{\rho}_1 \end{bmatrix} = \begin{bmatrix} -A_1 \frac{\rho_0 \lambda_1 \pi_1}{2V_1} & 0 & -A_1 \frac{\rho_1^2}{\kappa} \\ 0 & -A_2 \frac{\rho_0 \lambda_2 \pi_2}{2V_2} & A_2 \frac{\rho_1^2}{\kappa} \\ A_1 \frac{\rho_1^2}{\kappa} & -A_2 \frac{\rho_1^2}{\kappa} & 0 \end{bmatrix} \begin{bmatrix} \partial_{\pi_1} H \\ \partial_{\pi_2} H \\ \partial_{\rho_1} H \end{bmatrix}$$

$$+ \begin{bmatrix} A_1 & 0 \\ 0 & -A_2 \\ 0 & 0 \end{bmatrix} \begin{bmatrix} P_{11} \\ P_{22} \end{bmatrix} \quad (21a)$$

$$\begin{bmatrix} Q_{11} \\ -Q_{22} \end{bmatrix} = \begin{bmatrix} A_1 & 0 & 0 \\ 0 & -A_2 & 0 \end{bmatrix} \begin{bmatrix} \partial_{\pi_1} H \\ \partial_{\pi_2} H \\ \partial_{\rho_1} H \end{bmatrix} \quad (21b)$$

where Q_{11} and Q_{22} are the inlet and outlet volumetric flows of fluid channel, P_{11} and P_{22} the corresponding inlet and outlet pressures, and the total energy is given by

$$H = \kappa \beta_S \left(\frac{\rho_1 - \rho_0 (1 + \ln(\rho_1/\rho_0))}{\rho_1 \rho_0} \right) + \sum_{i=1}^{2} \frac{1}{2} C_{xi} \pi_i^2 \quad (22)$$

3. SCALABLE MODEL

The model propose in (21) describes the behavior of two fluid sections. However, the use of node model in (17) can be extended to interconnect n fluid sections. In this section, we expand the models in (10) and (17) to describe n fluid sections and $n - 1$ nodes, and define the interconnections to obtain the fluid channel model.

First, for n fluid sections we define $\pi = [\pi_1, \pi_2, \cdots, \pi_n]^T$ as the momenta vector and $K = \sum_{i=1}^{n} K_i$ as the total kinetic energy, from (10) we can describe the fluid behavior in n channel sections as

$$\dot{\pi} = -R \partial_\pi K + [g_{\pi 1} \ -g_{\pi 2}] \begin{bmatrix} u_{\pi 1} \\ u_{\pi 2} \end{bmatrix} + g \begin{bmatrix} P_1 \\ P_2 \end{bmatrix} \quad (23a)$$

$$\begin{bmatrix} y_{\pi 1} \\ y_{\pi 2} \end{bmatrix} = \begin{bmatrix} g_{\pi 1}^T \\ -g_{\pi 2}^T \end{bmatrix} \partial_\pi K \quad (23b)$$

$$\begin{bmatrix} Q_1 \\ -Q_2 \end{bmatrix} = g^T \partial_\pi K \quad (23c)$$

where P_1 and P_2 are the external pressures in the inlet and outlet boundary sections, respectively, Q_1 and Q_2 the corresponding volumetric flows, $u_{\pi 1} = [P_{12}, \cdots, P_{1n}]^T$ is the inlet pressure vector, $u_{\pi 2} = \left[P_{21}, \cdots, P_{2(n-1)} \right]^T$ is the outlet pressure vector, $y_{\pi 1} = [Q_{12}, \cdots, Q_{1n}]^T$ and $y_{\pi 2} = \left[Q_{21}, \cdots, Q_{2(n-1)} \right]^T$ are the internal inlet and outlet volumetric flow vectors, $R \in \mathbb{R}^{n \times n}$ is the dissipation matrix associated with energy losses by the geometry changes, and matrices $g \in \mathbb{R}^{n \times 2}$ and $\{g_{\pi 1}, g_{\pi 2}\} \in \mathbb{R}^{n \times (n-1)}$ are given by

$$g_{\pi 1} = \begin{bmatrix} 0 & 0 & \cdots & 0 \\ A_2 & 0 & \cdots & 0 \\ 0 & A_3 & \cdots & 0 \\ \vdots & \vdots & \ddots & \vdots \\ 0 & 0 & \cdots & A_n \end{bmatrix} \quad g_{\pi 2} = \begin{bmatrix} A_1 & 0 & \cdots & 0 \\ 0 & A_2 & \cdots & 0 \\ \vdots & \vdots & \ddots & \vdots \\ 0 & 0 & \cdots & A_{n-1} \\ 0 & 0 & \cdots & 0 \end{bmatrix}$$

$$g = \begin{bmatrix} A_1 & 0 \\ \mathbf{0} & \mathbf{0} \\ 0 & -A_n \end{bmatrix}$$

where $\mathbf{0}$ is a zero matrix of suitable dimensions. Matrix R will be define in Section 4.

Now, to obtain a description of the $n - 1$ nodes we define $\rho = [\rho_1, \rho_2, \cdots, \rho_{n-1}]^T$ as the density vector and $E = \sum_{j=1}^{n-1} E_j$ as the fluid potential energy. Thus, from (17) the behavior of nodes in the fluid channel is given by

$$\dot{\rho} = \mathbf{0} \partial_\rho E + [g_\rho \ -g_\rho] \begin{bmatrix} u_{\rho 1} \\ u_{\rho 2} \end{bmatrix} \quad (24a)$$

$$\begin{bmatrix} y_{\rho 1} \\ y_{\rho 2} \end{bmatrix} = \begin{bmatrix} g_\rho^T \\ -g_\rho^T \end{bmatrix} \partial_\rho E \quad (24b)$$

where $u_{\rho 1}$ is the inlet flow vector of nodes and $u_{\rho 2}$ is the outlet flow vector, $y_{\rho 1}$ and $y_{\rho 2}$ are the inlet and outlet node pressures, respectively, and $g_\rho \in \mathbb{R}^{(n-1) \times (n-1)}$ is given by

$$g_\rho = \begin{bmatrix} \rho_1^2/k & 0 & \cdots & 0 \\ 0 & \rho_2^2/k & \cdots & 0 \\ \vdots & \vdots & \ddots & \vdots \\ 0 & 0 & \cdots & \rho_{n-1}^2/k \end{bmatrix}$$

Note that the input and output ports of nodes model in (24) are compatible with the corresponding ports of sections model in (23). Thus, we can define the following interconnection rule

$$\begin{bmatrix} u_{\pi 1} \\ u_{\pi 2} \\ u_{\rho 1} \\ u_{\rho 2} \end{bmatrix} = \begin{bmatrix} \mathbf{0} & \mathbf{0} & \mathbf{0} & -I \\ \mathbf{0} & \mathbf{0} & I & \mathbf{0} \\ \mathbf{0} & -I & \mathbf{0} & \mathbf{0} \\ I & \mathbf{0} & \mathbf{0} & \mathbf{0} \end{bmatrix} \begin{bmatrix} y_{\pi 1} \\ y_{\pi 2} \\ y_{\rho 1} \\ y_{\rho 2} \end{bmatrix} \quad (25)$$

Finally, using (23), (24) and (25), we obtain that fluid behavior in a channel with irregular geometries is given by

$$\begin{bmatrix} \dot{\pi} \\ \dot{\rho} \end{bmatrix} = \begin{bmatrix} -R & J \\ -J^T & \mathbf{0} \end{bmatrix} \begin{bmatrix} \partial_\pi H \\ \partial_\rho H \end{bmatrix} + \begin{bmatrix} g \\ \mathbf{0} \end{bmatrix} \begin{bmatrix} P_1 \\ P_2 \end{bmatrix} \tag{26a}$$

$$\begin{bmatrix} Q_1 \\ -Q_2 \end{bmatrix} = \begin{bmatrix} g^T & \mathbf{0} \end{bmatrix} \begin{bmatrix} \partial_\pi H \\ \partial_\rho H \end{bmatrix} \tag{26b}$$

where P_1 and P_2 are the boundary pressures of fluid channel, Q_1 and Q_2 are the corresponding intlet and outlet volumetric flows, $J = (g_{\pi 1} - g_{\pi 2}) g_\rho^T$ and the total energy is given by

$$H = \sum_{i=1}^{n} \frac{1}{2} \frac{\pi_i^2}{\rho_0 V_i} + \sum_{j=1}^{n-1} \kappa \beta_S \left(\frac{\rho_j - \rho_0 \left(1 + \ln(\rho_j/\rho_0)\right)}{\rho_j \rho_0} \right) \tag{27}$$

4. DEFINITION OF LOSS FACTORS

The definition of the loss factor λ_i depends of geometry variation of the channel. In literature, we can found studies where is analyzed the loss factor for direction changes in the channel (Haidar, 1995; Villegas-León et al., 2016), channel contractions and expansions (Mulley, 2004; Crane, 2013), and T and Y junctions (Bassett et al., 2001; Nikita et al., 2015; Oka and Itō, 2005; Pérez-García et al., 2010). In this work we consider only the loss factors associated with sudden expansions and contractions.

In a sudden expansion, when the fluid enters in a section with enlarged cross-sectional area a jet is formed as the fluid separates from the wall of the small channel. This jet expands until it fills the entire area and some fluid break away and circulates in the corner of the expanded section (Brodkey and Hershey, 2003; Mulley, 2004). In this case the loss factor is given by

$$\lambda_i^e = \left(1 - \frac{A_i}{A_{i+1}}\right)^2 \tag{28}$$

In a sudden contraction, the flow behavior is different that in an expansion. Given the are reduction of the channel, the fluid accelerates as it enters the small section and occurs a well-known phenomena called *vena contracta*. According to Mulley (2004) the loss factor in sudden contraction is given by

$$\lambda_i^c = \frac{1}{2}\left(1 - \frac{A_i}{A_{i-1}}\right) \tag{29}$$

According to Brodkey and Hershey (2003), the loss factor in the entrance flow depends of the entrance channel geometry and is less than 0.78, and loss factor associated width the exit flow is equal to 1.

Then, from above considerations for energy losses associated with the internal irregular geometries, the dissipation matrix in (26) is given by

$$R = \begin{bmatrix} A_1 \frac{\rho_0 \lambda_1 \pi_1}{2V_1} & 0 & \cdots & 0 \\ 0 & A_2 \frac{\rho_0 \lambda_2 \pi_2}{2V_2} & \cdots & 0 \\ \vdots & \vdots & \ddots & \vdots \\ 0 & 0 & \cdots & A_n \frac{\rho_0 \pi_n}{2V_n} \end{bmatrix}$$

where each $\lambda_i, i \in [1, n-1]$ are define by λ_i^e or λ_i^c depending of the internal geometry and the loss factor in the last section is given by $\lambda_n = 1$.

In cases where in the internal losses are neglected the dissipation matrix is given loss factor of the the last section, i.e.,

$$R = \begin{bmatrix} \mathbf{0} & \mathbf{0} \\ \mathbf{0} & A_n \frac{\rho_0 \pi_n}{2V_n} \end{bmatrix} \tag{30}$$

5. NUMERICAL EXAMPLES

In this section we presents numerical simulations for application examples of the model proposed in (26) using ODE15s solver of MATLAB software. In these examples we consider as fluid an airflow whose density is given by $\rho_0 = 1.1376 kg/m^3$ at $35°C$ and bulk modulus $\beta_S = 142 \times 10^3 Pa$.

Nest, we presents 2 examples. In Example 1 we study a pipe with uniform cross sectional area using 4 fluid section, where as the geometry no change the internal dissipations are neglected. In Example 2, we analyze a pipe width 2 area changes, one contraction and one expansion, using 6 fluid sections and including the dissipative effects associated with geometry changes.

On the other hand, as has been mentioned in Section 1, in the practice a fluid is considered incompressible if the density variations are negligible. Other assumption in incompressible fluids is that the potential energy of the flow is negligible in comparison with the corresponding kinetic energy. To evaluate that the model proposed in (26) satisfy these considerations, we analyze the density changes $\Delta \rho_i$ in each node using

$$\Delta \rho_i = 100 \frac{\rho_j - \rho_0}{\rho_0} \tag{31}$$

and the normalized kinetic and potential energies in the system, $\bar{K}$ and $\bar{E}$, respectively, where

$$\bar{K} = \frac{\sum_{i=1}^{n} \frac{1}{2} \frac{\pi_i^2}{\rho_0 V_i}}{H} \tag{32}$$

$$\bar{E} = \frac{\sum_{j=1}^{n-1} \kappa \beta_S \left(\frac{\rho_j - \rho_0 (1 + \ln(\rho_j/\rho_0))}{\rho_j \rho_0} \right)}{H} \tag{33}$$

Example 1. A pipe of 4 sections with equal cross-sectional area   Consider a pipe with a transversal area A_0 and length L, we divide this pipe in 4 sections with volume $V_0 = A_0 L/4$. Thus, the matrices associated with the port-Hamiltonian model in (26) are given by

$$R = \begin{bmatrix} 0 & 0 & 0 & 0 \\ 0 & 0 & 0 & 0 \\ 0 & 0 & 0 & 0 \\ 0 & 0 & 0 & s_4 \frac{\lambda \pi_4}{V_0} \end{bmatrix} \qquad G = \begin{bmatrix} A_0 & 0 \\ 0 & 0 \\ 0 & 0 \\ 0 & -A_0 \end{bmatrix}$$

$$J = \frac{A_0}{k} \begin{bmatrix} -\rho_1^2 & 0 & 0 \\ \rho_1^2 & -\rho_2^2 & 0 \\ 0 & \rho_2^2 & -\rho_3^2 \\ 0 & 0 & \rho_3^2 \end{bmatrix}$$

Setting $A_0 = 1 \times 10^{-4} m^2$, $L = 1 \times 10^{-3}m$, $\kappa = 1 \times 10^{-10} kg$, and $P_1 = 800 Pa$ and $P_2 = 0 Pa$, we obtain the simulation results that shown in Figure 4. Note that the momenta presents a fast convergence to an uniform behavior in all sections (Figure 4.a). The density variation
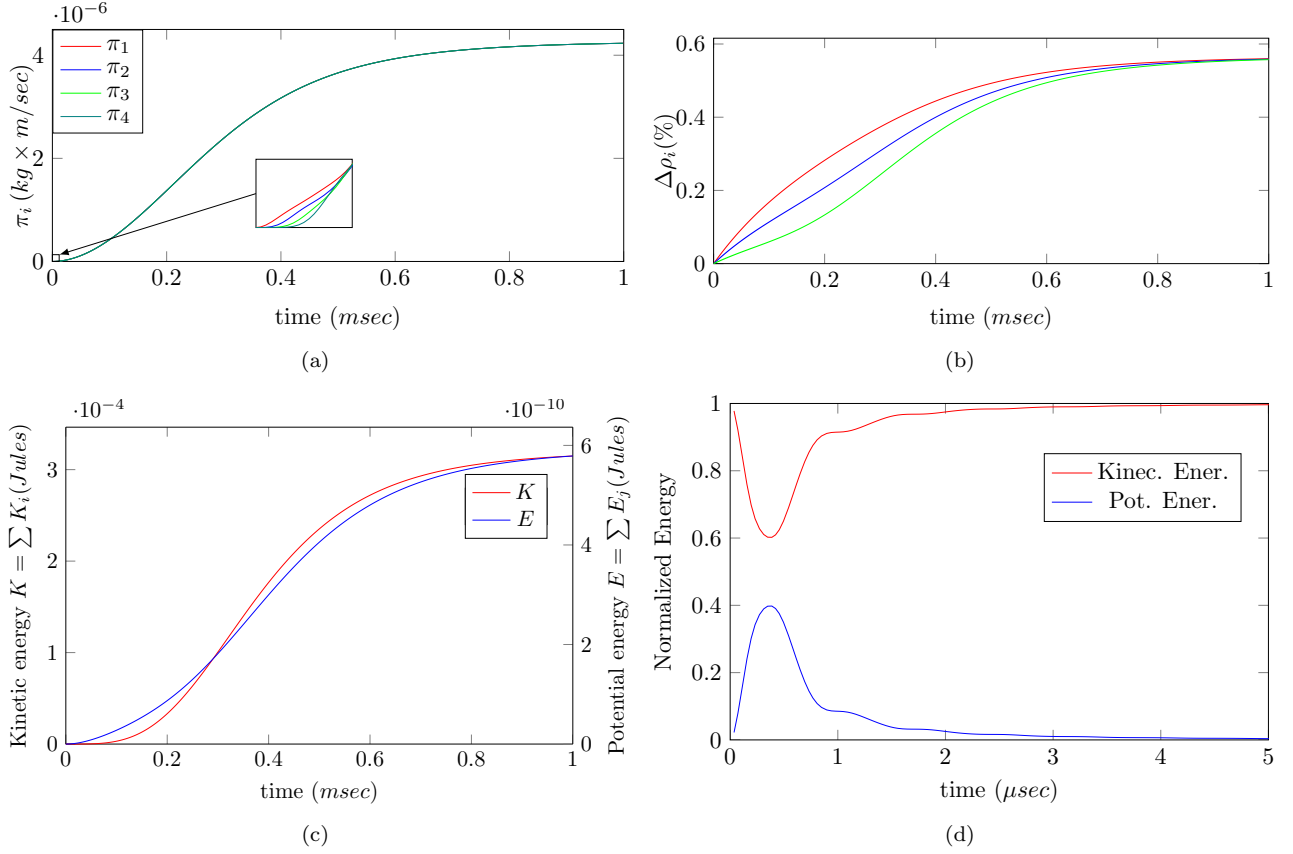
Fig. 4. Simulation results for example 1. (a) Momentum behavior in each fluid section, (b) Density variation in each node, (c) Behavior of kinetic (red line) and potential (blue line) energies in Joules, (d) Normalized kinetic (red line) and potential (blue line) energies
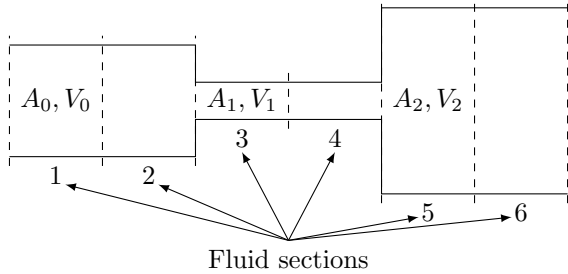
Fig. 5. Fluid channel with irregular geometry

is less than 0.6% (Figure 4.b), i.e., the density varies in concordance with Assumption 1, that traditionally can be neglected. Finally, the energy behavior is shown, where the potential energy is significant only in the first moments of simulation (Figure 4.d), later kinetic energy is dominant, being greater than potential energy in a scale of 10^6 times (Figure 4.c). All these results are in concordance with the conditions used traditionally to assume the incompressible hypothesis.

Example 2. A pipe with different cross sectional areas
Consider a pipe that present contraction and expansion section, as shown in Figure 5. The matrices of port-Hamiltonian formulation in (26) are given by

$$R = \begin{bmatrix} 0 & 0 & 0 & 0 & 0 & 0 \\ 0 & s_2\dfrac{\lambda_2\pi_2}{V_0} & 0 & 0 & 0 & 0 \\ 0 & 0 & 0 & 0 & 0 & 0 \\ 0 & 0 & 0 & s_4\dfrac{\lambda_4\pi_4}{V_1} & 0 & 0 \\ 0 & 0 & 0 & 0 & 0 & 0 \\ 0 & 0 & 0 & 0 & 0 & s_6\dfrac{\lambda_6\pi_6}{V_2} \end{bmatrix}$$

$$J = \frac{1}{k} \begin{bmatrix} -A_0\rho_1^2 & 0 & 0 & 0 & 0 \\ A_0\rho_1^2 & -A_0\rho_2^2 & 0 & 0 & 0 \\ 0 & A_1\rho_2^2 & -A_1\rho_3^2 & 0 & 0 \\ 0 & 0 & A_1\rho_3^2 & -A_1\rho_4^2 & 0 \\ 0 & 0 & 0 & A_2\rho_4^2 & -A_2\rho_5^2 \\ 0 & 0 & 0 & 0 & A_2\rho_5^2 \end{bmatrix}$$

$$G = \begin{bmatrix} A_0 & 0 & 0 & 0 & 0 \\ 0 & 0 & 0 & 0 & -A_2 \end{bmatrix}^T$$

where $\lambda_2 = (1/2)(1 - A_1/A_0)$ and $\lambda_2 = (1 - A_1/A_2)^2$ are the loss factors associated with a sudden pipe contraction and expansion Hager (2010), respectively, and $\lambda_6 = 1$ is the loss factor when the airflow leaves of the pipe.

Setting $A_0 = 1 \times 10^{-4}m^2$, $A_1 = 0.5 \times 10^{-4}m^2$, $A_2 = 2 \times 10^{-4}m^2$, $V_0 = 1 \times 10^{-7}m^3$, $V_1 = 0.5 \times 10^{-7}m^3$, $V_2 = 2 \times 10^{-7}m^3$,, $\kappa = 1 \times 10^{-10}kg$, and $P_1 = 800Pa$ and $P_2 = 0Pa$, we obtain the simulation results that shown in Figure 5. The top row shows the air momentum and velocity behavior in each section. Note that the momenta presents

a fast convergence to the same signal for all sections, and the velocities depends of the section area. The middle row shows the density behavior. Note that the density variation is less than 1 percent, i.e., the density varies in concordance with Assumption 1. Finally, in bottom row the energy behavior is shown, where the potential energy is significant only in the first moments of simulation, later the kinetic energy is dominant.

REFERENCES

Altmann, R. and Schulze, P. (2017). A port-Hamiltonian formulation of the Navier–Stokes equations for reactive flows. *Systems & Control Letters*, 100, 51–55. doi:10.1016/j.sysconle.2016.12.005.

Bassett, M.D., Winterbone, D.E., and Pearson, R.J. (2001). Calculation of steady flow pressure loss coefficients for pipe junctions. *Proceedings of the I MECH E Part C Journal of Mechanical Engineering Scienc*, 215(8), 861–881. doi:10.1243/0954406011524199.

Bird, R.B., Stewart, W.E., Lightfoot, E.N., and Klingenberg, D.J. (2014). *Introductory Transport Phenomena*. Jhon Wiley & Sons, United States of America.

Bourantas, G.C., Cheeseman, B.L., Ramaswamy, R., and Sbalzarini, I.F. (2016). Using DC PSE operator discretization in eulerian meshless collocation methods improves their robustness in complex geometries. *Computers & Fluids*, 136, 285–300. doi:10.1016/j.compfluid.2016.06.010.

Brodkey, R. and Hershey, H. (2003). *Transport Phenomena: A Unified Approach*. Chemical engineering series. Brodkey Publishing.

Cal, I.R., Cercos-Pita, J.L., and Duque, D. (2017). The incompressibility assumption in computational simulations of nasal airflow. *Computer Methods in Biomechanics and Biomedical Engineering*, 20(8), 853–868. doi:10.1080/10255842.2017.1307343.

Cisonni, J., Van Hirtum, A., Pelorson, X., and Willems, J. (2008). Theoretical simulation and experimental validation of inverse quasi-one-dimensional steady and unsteady glottal flow models. *The Journal of the Acoustical Society of America*, 124(1), 535–545. doi:10.1121/1.2931959.

Comer, J.K., Kleinstreuer, C., and Zhang, Z. (2001). Flow structures and particle deposition patterns in double-bifurcation airway models. Part 1. Air flow fields. *Journal of Fluid Mechanics*, 435. doi:10.1017/S0022112001003809.

Crane (2013). Flow of Fluids Through Valves, Fittings and Pipe. Technical Paper No 410.

Darbandi, M. and Naderi, A. (2006). Multiblock hybrid grid finite volume method to solve flow in irregular geometries. *Computer Methods in Applied Mechanics and Engineering*, 196(1-3), 321–336. doi:10.1016/j.cma.2006.04.005.

Guidoboni, G., Glowinski, R., Cavallini, N., Canic, S., and Lapin, S. (2009). A kinematically coupled time-splitting scheme for fluid–structure interaction in blood flow. *Applied Mathematics Letters*, 22(5), 684–688. doi:10.1016/j.aml.2008.05.006.

Hager, W.H. (2010). Losses in Flow. In *Wastewater Hydraulics*, 17–54. Springer Berlin Heidelberg, Berlin, Heidelberg, second edition. doi:10.1007/978-3-642-11383-3_2.

Haidar, N. (1995). Prediction of compressible flow pressure losses in 30–150 deg sharp-cornered bends. *Journal of Fluids Engineering*, 117(4), 589. doi:10.1115/1.2817306.

Johnson, R. (1998). *The Handbook of Fluid Dynamics*. Mechanical engineering. Springer Berlin Heidelberg.

Kotyczka, P. (2013). Discretized models for networks of distributed parameter port-Hamiltonian systems. In *Proceedings of the 8th International Workshop on Multidimensional Systems (nDS13)*, 63–67. VDE, Erlangen, Germany.

Kotyczka, P. and Maschke, B. (2017). Discrete port-Hamiltonian formulation and numerical approximation for systems of two conservation laws. *at - Automatisierungstechnik*, 65(5), 308–322. doi:10.1515/auto-2016-0098.

Morrison, P.J. (1998). Hamiltonian description of the ideal fluid. *Reviews of Modern Physics*, 70(2), 467–521. doi:10.1103/RevModPhys.70.467.

Morrison, P., Lebovitz, N.R., and Biello, J.A. (2009). The Hamiltonian description of incompressible fluid ellipsoids. *Annals of Physics*, 324(8), 1747–1762. doi:10.1016/j.aop.2009.04.003.

Mulley, R. (2004). *Flow of Industrial Fluids: Theory and Equations*. CRC Press.

Nikita, C., Hardalupas, Y., and Taylor, A. (2015). Study of Pressure Losses of Unsteady Compressible Flows in Three- Way Junctions. In *SAE Technical Paper 2015-24-2399*. doi:10.4271/2015-24-2399.

Oka, K. and Itō, H. (2005). Energy Losses at Tees With Large Area Ratios. *Journal of Fluids Engineering*, 127(1), 110. doi:10.1115/1.1852475.

Pérez-García, J., Sanmiguel-Rojas, E., and Viedma, A. (2010). New coefficient to characterize energy losses in compressible flow at T-junctions. *Applied Mathematical Modelling*, 34(12), 4289–4305. doi:10.1016/j.apm.2010.05.005.

Sharatchandra, M.C. and Rhode, D.L. (1994). New, strongly conservative finite-volume formulation for fluid flows in irregular geometries using contravariant velocity components: Part 1. theory. *Numerical Heat Transfer, Part B: Fundamentals*, 26(1), 39–52. doi:10.1080/10407799408914915.

Trenchant, V., Hu, W., Ramirez, H., and Gorrec, Y.L. (2018a). Structure Preserving Finite Differences in Polar Coordinates for Heat and Wave Equations. *IFAC-PapersOnLine*, 51(2), 571–576. doi:10.1016/j.ifacol.2018.03.096.

Trenchant, V., Ramirez, H., Le Gorrec, Y., and Kotyczka, P. (2018b). Finite differences on staggered grids preserving the port-Hamiltonian structure with application to an acoustic duct. *Journal of Computational Physics*, 373, 673–697. doi:10.1016/j.jcp.2018.06.051.

van der Schaft, A.J. and Maschke, B.M. (2002). Hamiltonian formulation of distributed-parameter systems with boundary energy flow. *Journal of Geometry and Physics*, 42(1-2), 166–194. doi:10.1016/S0393-0440(01)00083-3.

Van der Schaft, A. (2017). *L2-Gain and Passivity Techniques in Nonlinear Control*. Communications and Control Engineering. Springer International Publishing, Cham, 3rd edition. doi:10.1007/978-3-319-49992-5.

Van der Schaft, A. and Jeltsema, D. (2014). Port-Hamiltonian Systems Theory: An Introductory
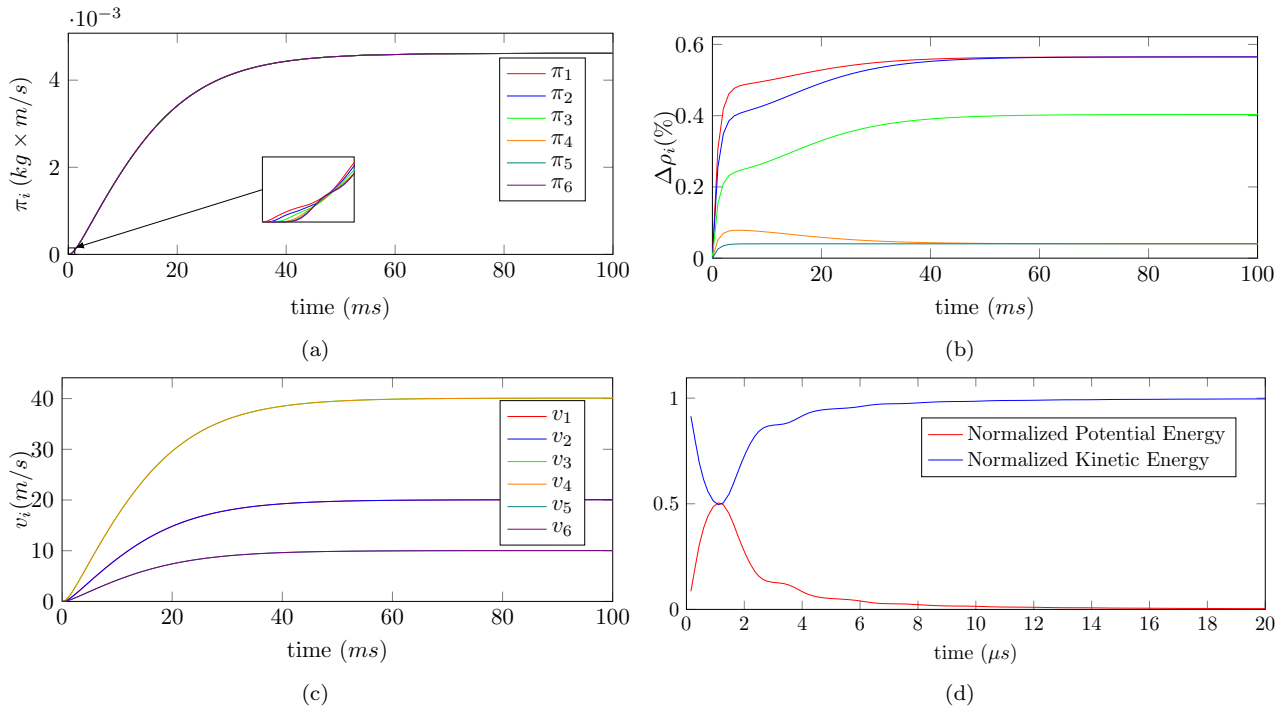
Fig. 6. Simulation results for example 2. (a) Momentum behavior in each fluid section, (b) Density variation in each node, (c) Behavior of kinetic (red line) and potential (blue line) energies in Joules, (d) Normalized kinetic (red line) and potential (blue line) energies

Overview. *Foundations and Trends® in Systems and Control*, 1(2-3), 173–378. doi:10.1561/2600000002.

Villegas-León, J.J., López-Lambraño, A.A., Morales-Nava, J.G., Pliego-Díaz, M., Fuentes, C., and López-Ramos, A. (2016). Equations to determine energy losses in sudden and gradual change of direction. In J. Klapp, A. López, L.D.G. Sigalotti, G. Ruiz-Chavarría, and A. Medina (eds.), *Recent Advances in Fluid Dynamics with Environmental Applications*, Environmental Science and Engineering, 465–475. Springer International Publishing Switzerland. doi:10.1007/978-3-319-27965-7_33.

Wu, Z. and Cao, Y. (2015). Numerical simulation of flow over an airfoil in heavy rain via a two-way coupled Eulerian–Lagrangian approach. *International Journal of Multiphase Flow*, 69, 81–92. doi:10.1016/j.ijmultiphaseflow.2014.11.006.